Supplementary Materials

Continuous-flow electrooxidation for scalable biomass upgrading over copper-supported CoFe Prussian blue analogues

Bowen Zhang[1,#], Tiantian Xiao[2,#], Cejun Hu[3,*], Zhichen Liu[1], Peng Chen[1], Zhengyu Zhao[1], Duanjing Lai[3], Jinming Huang[1], Hongwei Zhang[1,*], Xiaojun Bao[1,4], Pei Yuan[1,4,*]

[1]National Engineering Research Center of Chemical Fertilizer Catalyst, College of Chemical Engineering, Fuzhou University, Fuzhou 350108, Fujian, China.
[2]Joint School of National University of Singapore and Tianjin University, International Campus of Tianjin University, Binhai New City, Fuzhou 350207, Fujian, China.
[3]College of Materials Science and Engineering, Fuzhou University, Fuzhou 350108, Fujian, China.
[4]Qingyuan Innovation Laboratory, Quanzhou 362801, Fujian, China.
[#]Authors contributed equally.

[*]**Correspondence to:** Prof. Cejun Hu, College of Materials Science and Engineering, Fuzhou University, No. 2 Wulong Jiangbei Avenue, Fuzhou 350108, Fujian, China. E-mail: cejun_hu@fzu.edu.cn; Prof. Hongwei Zhang, Prof. Pei Yuan, National Engineering Research Center of Chemical Fertilizer Catalyst, College of Chemical Engineering, No. 2 Wulong Jiangbei Avenue, Fuzhou University, Fuzhou 350108, Fujian, China. E-mail: zhanghw@fzu.edu.cn; yuanpei@fzu.edu.cn

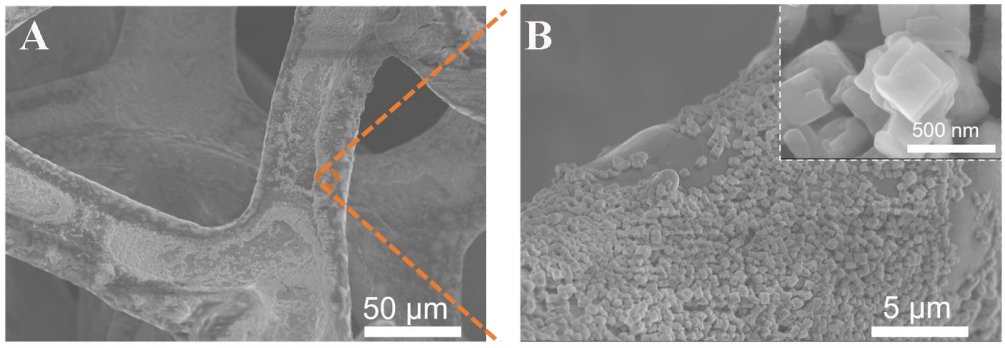

Supplementary Figure 1. (A and B) SEM images of CoFe PBA-CF.

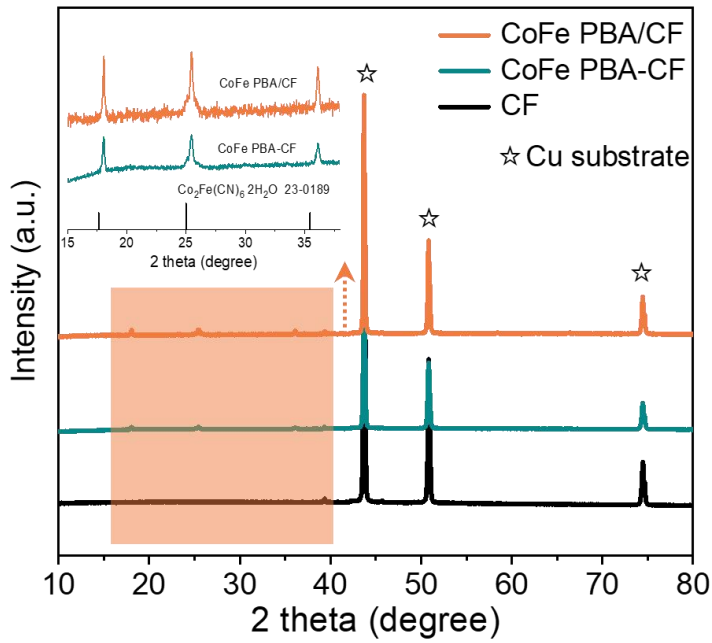

Supplementary Figure 2. XRD pattern of the CoFe PBA/CF and CoFe PBA-CF.

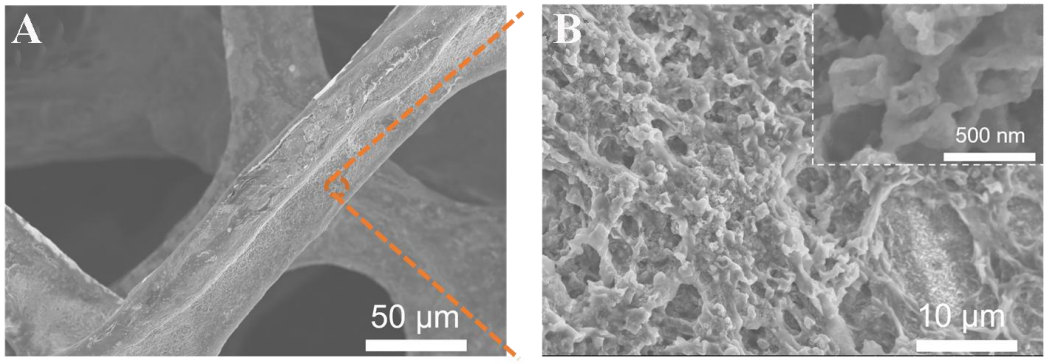

Supplementary Figure 3. (A and B) SEM images of CoFe PBA-CF after reconstruction in KOH solution.

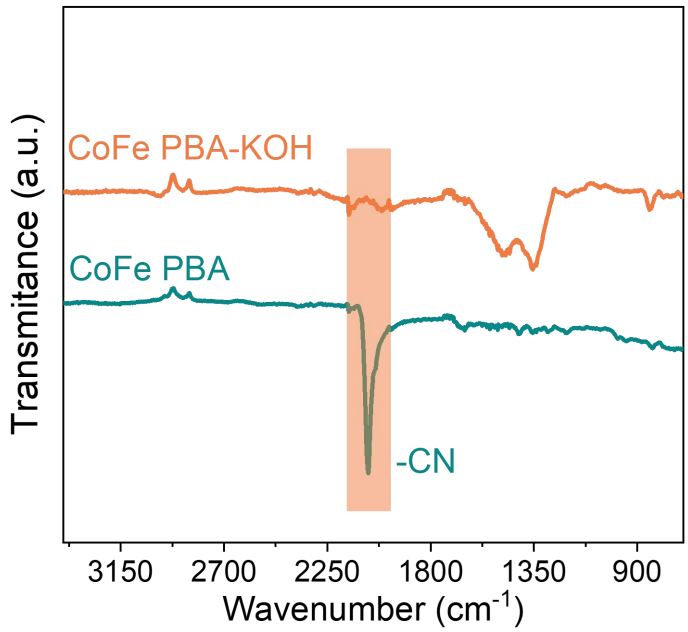

Supplementary Figure 4. FTIR patterns of the CoFe PBA/CF sample before and after reconstruction in KOH solution.

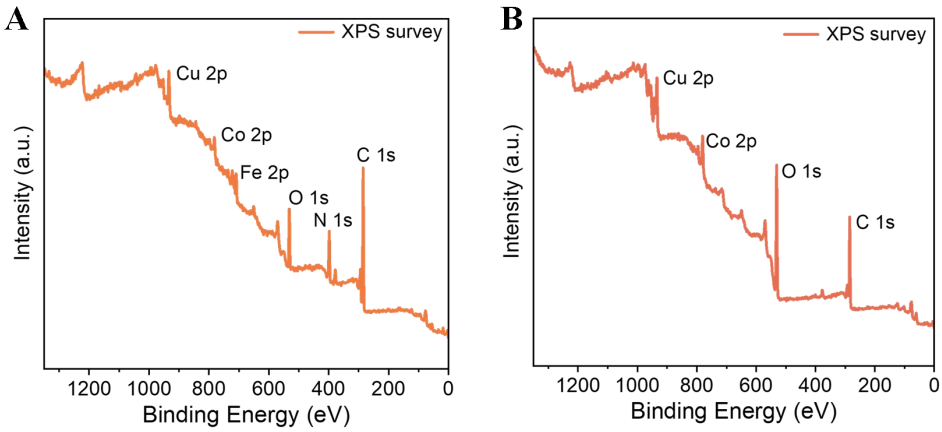

Supplementary Figure 5. XPS spectrum of CoFe PBA (A) before and (B) after reconstruction in KOH solution.

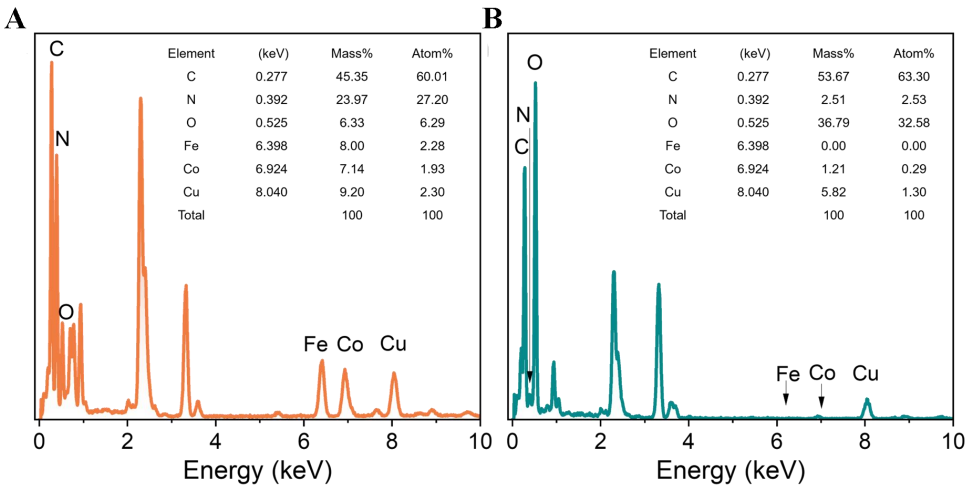

Supplementary Figure 6. EDS pattern of CoFe PBA/CF sample (A) before and (B) after reconstruction in KOH solution.

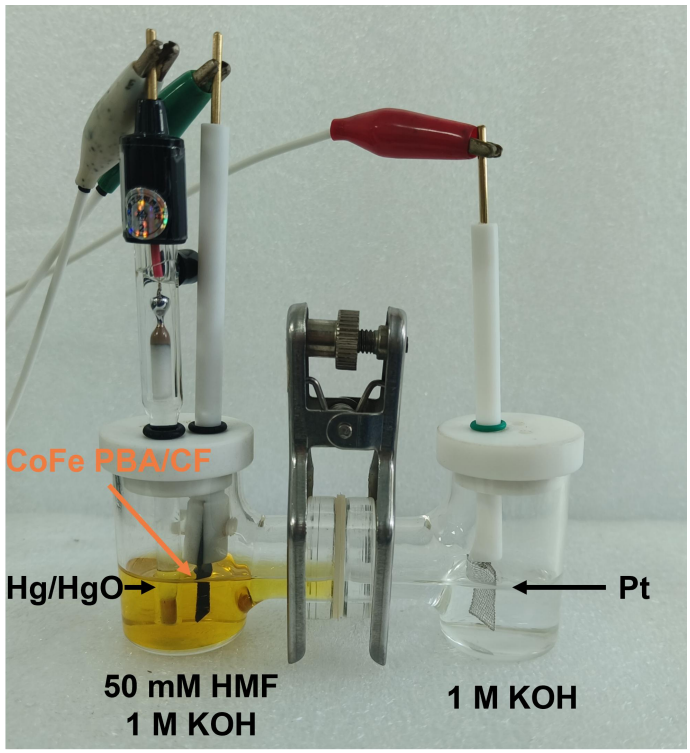

Supplementary Figure 7. Photographic image of H-type electrolytic cell for electrochemical HMFOR.

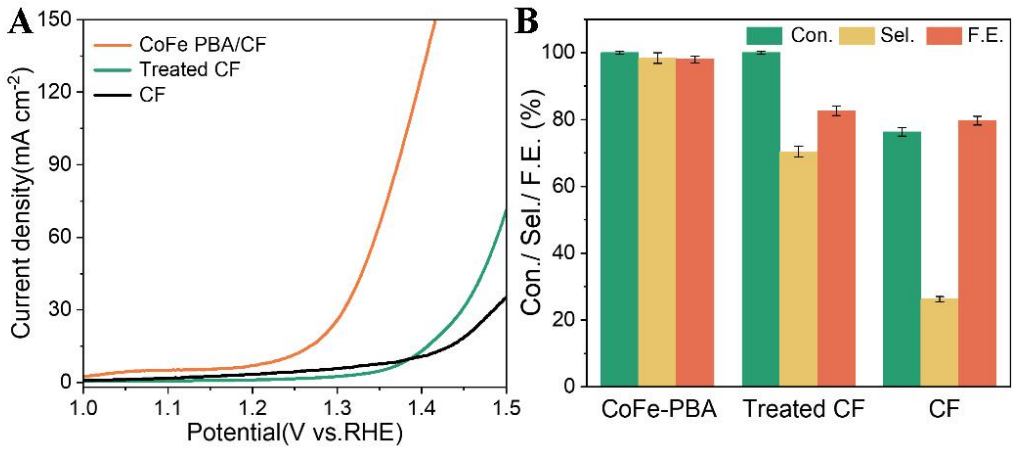

Supplementary Figure 8. (A) Polarization curves, and (B) a comparison of HMF conversion, FDCA yield, and FE between CoFe PBA/CF, hydrothermal CF, and CF.

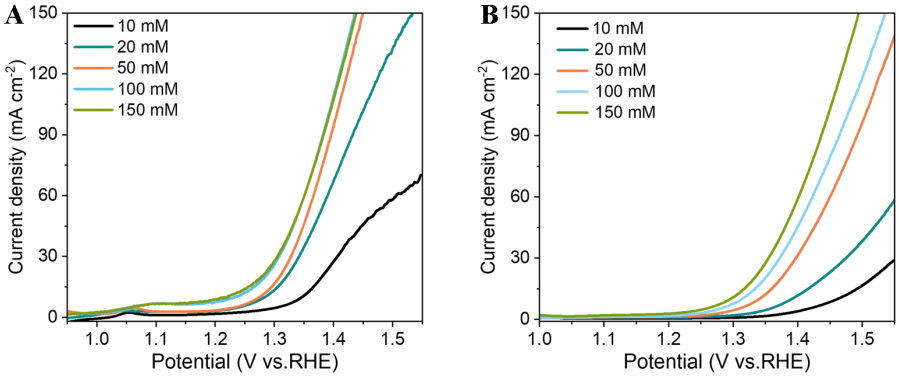

Supplementary Figure 9. Polarization curves of (A) CoFe PBA/CF and (B) CoFe PBA-CF with different HMF concentrations.

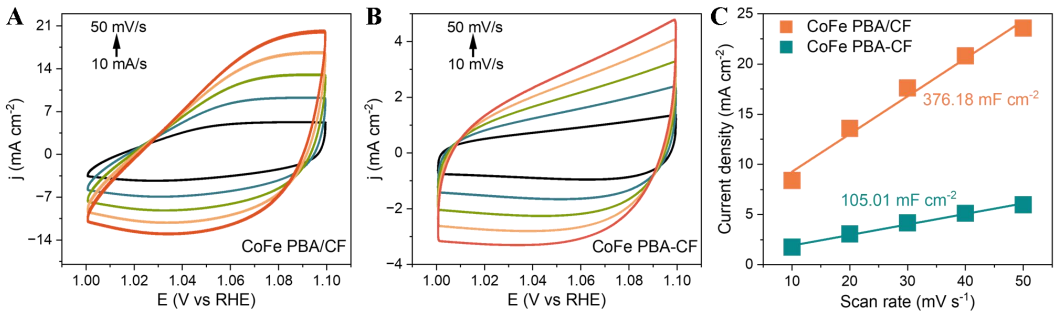

Supplementary Figure 10. CV curves of (A) CoFe PBA/CF and (B) CoFe PBA-CF at different scan rates from 10 mV/s to 50 mV/s, (C) the capacitive currents as a function of the scan rate (1.05 V *vs.* RHE).

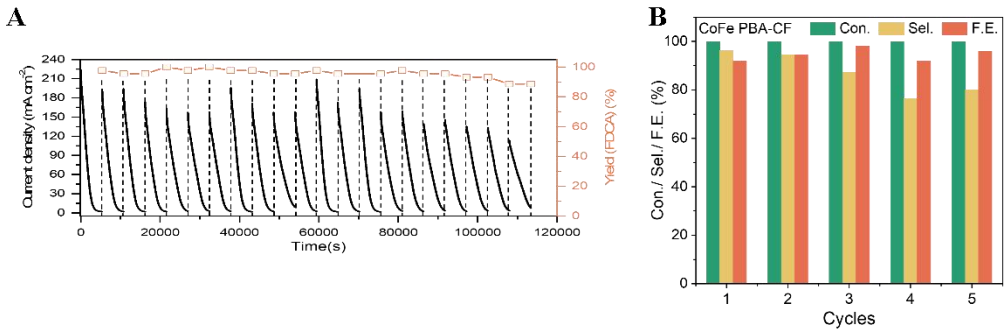

Supplementary Figure 11. (A) I-t curves and FDCA yield of CoFe PBA/CF at 1.45 V with the intermittent addition of 50 mM HMF; (B) HMF conversion, FDCA selectivity, and FE of CoFe PBA-CF at firstly 5 cycles.

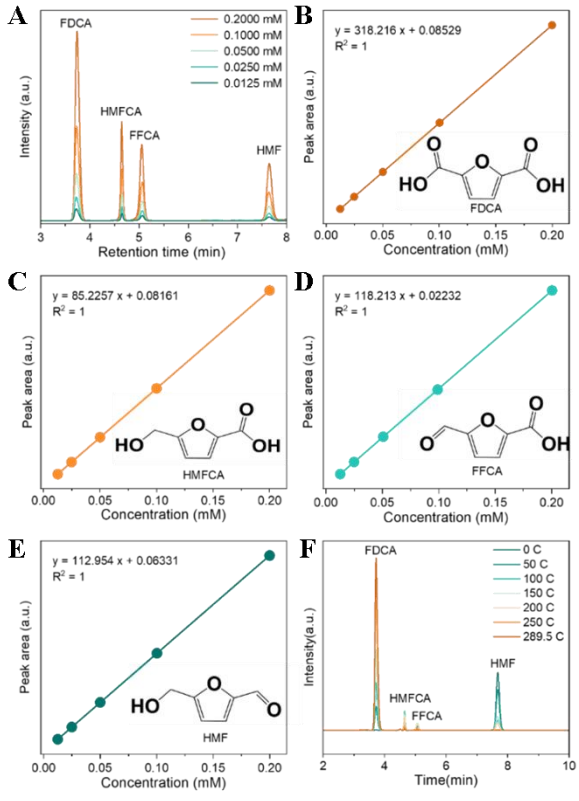

Supplementary Figure 12. (A) HPLC chromatograms and corresponding standard curves for (B) FDCA, (C) HMFCA, (D) FFCA and (E) HMF. (F) Concentration changes of the reactant and products during HMFOR at 1.45 V.

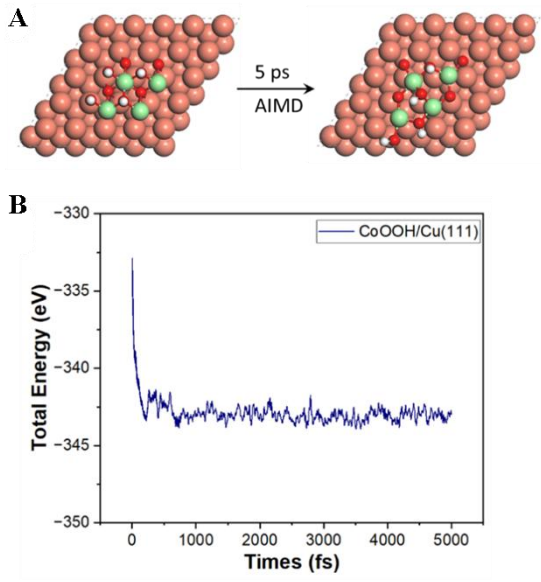

Supplementary Figure 13. (A) Top views of initial (0 ps) and final (5 ps) structure during AIMD simulation of CoOOH/Cu(111) under 298 K; (B) The total energy by performing the AIMD simulation in 5000 steps (the steps size was set to 1 fs).

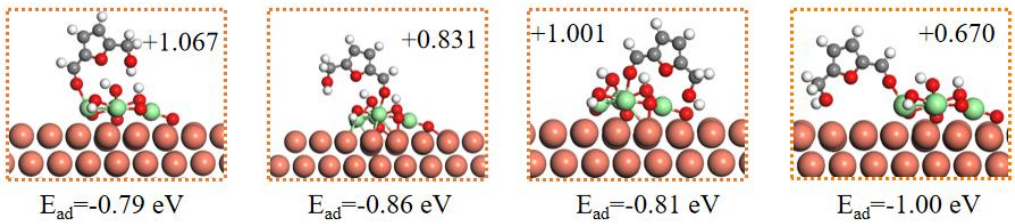

Supplementary Figure 14. The adsorption energies of HMF for different Co sites on CoOOH/Cu(111) surface.

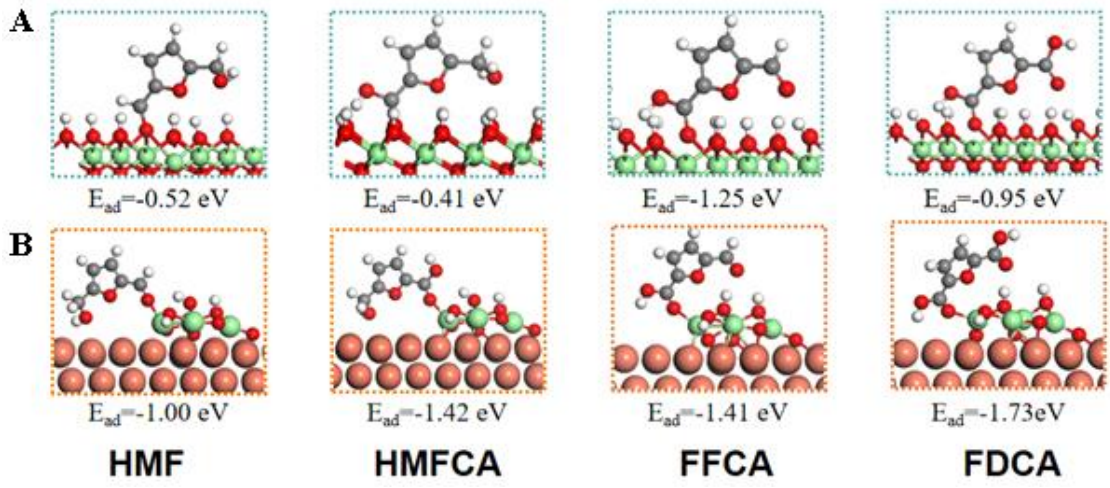

Supplementary Figure 15. The adsorption energies of surface species on (A) CoOOH and (B) CoOOH/Cu(111) surfaces.

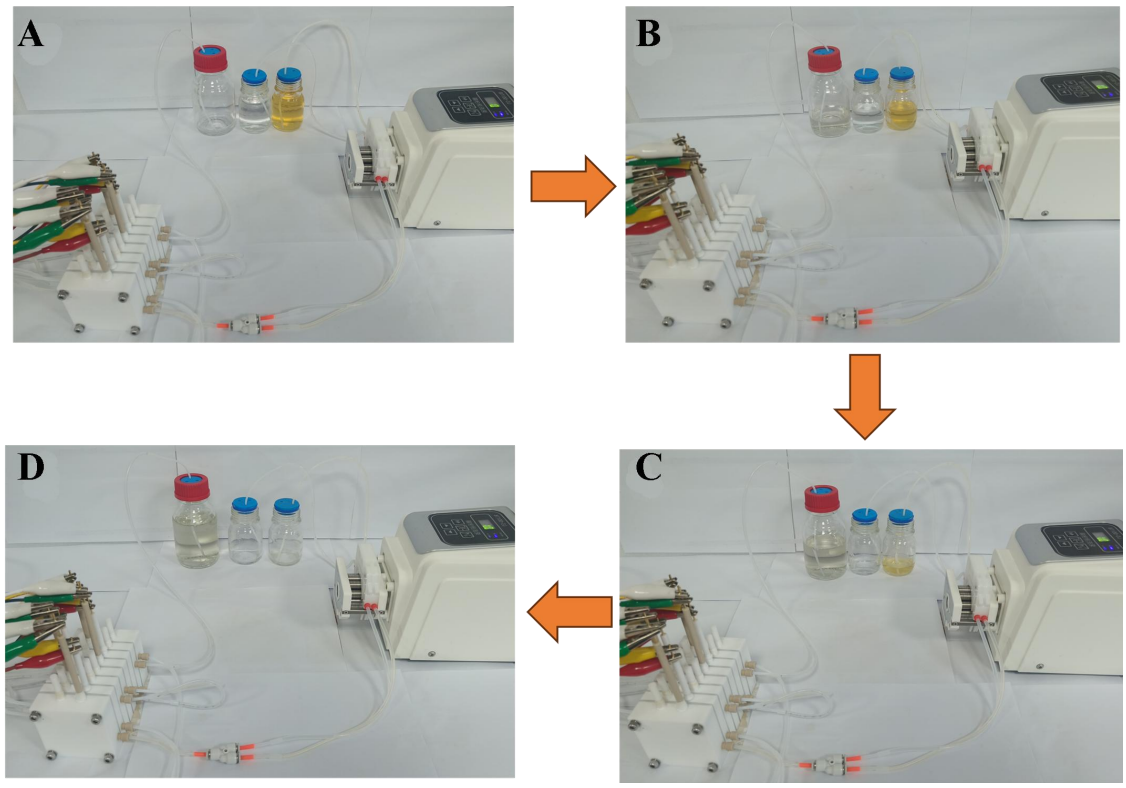

Supplementary Figure 16. (A-D) Photographic images of the continuous oxidation of high-concentration HMF to FDCA via the CFER.

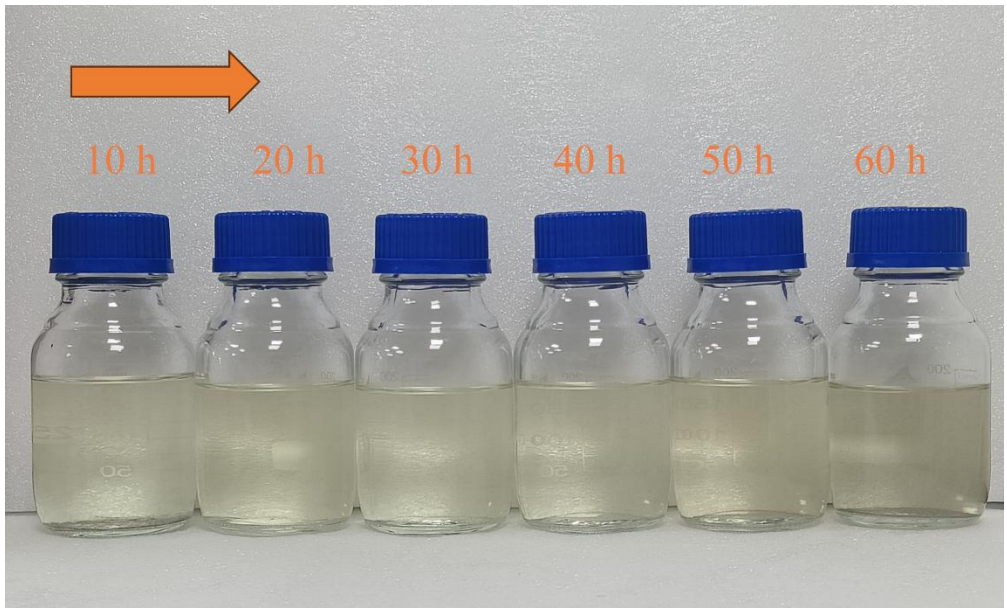

Supplementary Figure 17. A photographic image of the product solution during 60 hours of continuous electrolysis in the CFER.

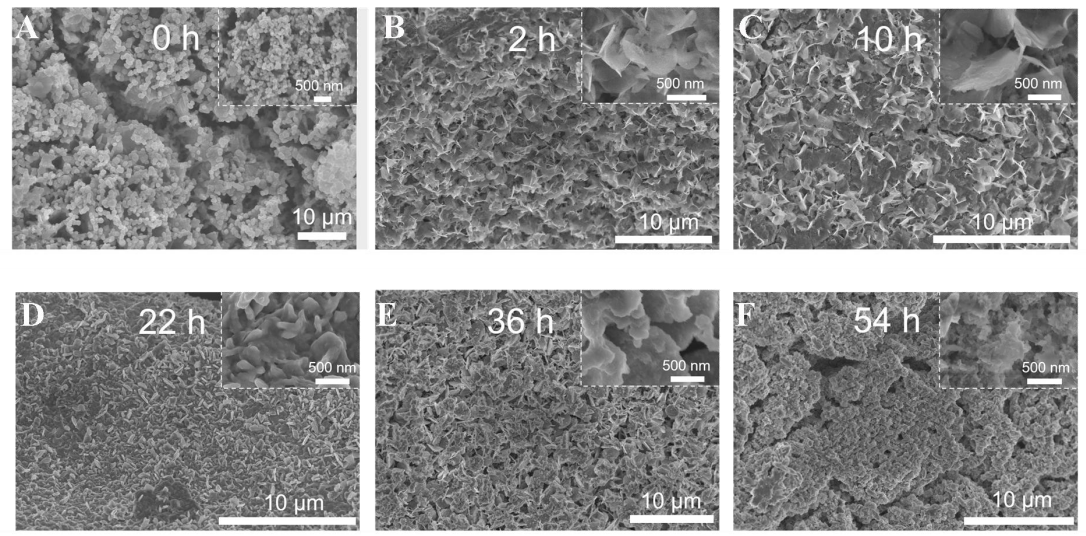

Supplementary Figure 18. (A-F) SEM images of CoFe PBA/CF after HMFOR cycles.

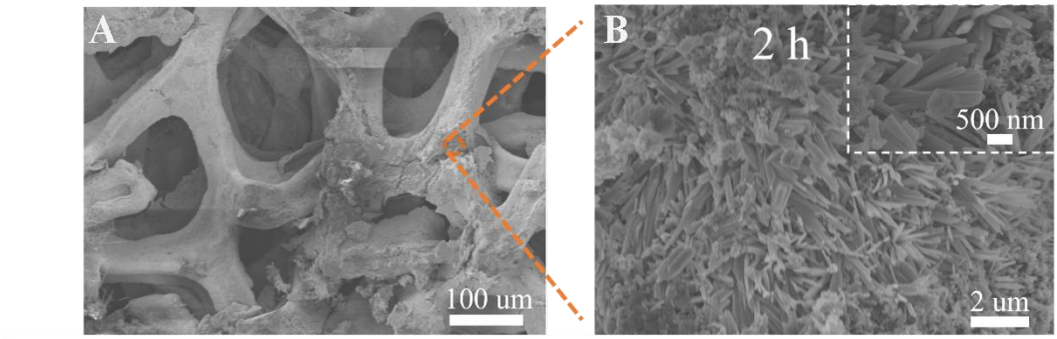

Supplementary Figure 19. (A and B) SEM images of CoFe PBA-CF after HMFOR.

Supplementary Table 1. ICP results of CoFe PBA/CF sample before and after electric-driven reconstruction

	Co (ppm)	Fe (ppm)	Ni:Fe ratio
Before reconstruction	18.53	18.27	1.01
After reconstruction	18.11	7.42	2.44

Supplementary Table 2. Comparisons of the catalytic performance of different catalysts

Electrocatalyst	Potential (V) @ j ($mA \cdot cm^{-2}$)	Potential applied (V)	C_{HMF} (mM)	FDCA yield (%)	Faradaic efficiency (%)	Ref.
CoFe PBA/CF	1.239 @ 10 1.335 @ 50	1.45	50	98.4	98	This work
Ni_3N@C	1.35 @ 10	1.45	10	98	99	[1]
$CuCo_2O_4$	1.39 @ 10	1.45	10	93.7	94	[2]
Ir-Co_3O_4	1.38 @ 10	1.42	10	98	98	[3]
NiCoFe-LDH/CFP	1.518 @ 10	1.54	10	84.9	90	[4]
$(FeCrCoNiCu)_3O_4$	1.52 @ 10	1.5	10	98	98	[5]
Vo-Co_3O_4	1.35 @ 10	1.47	10	91.9	88.1	[6]
CF-$Cu(OH)_2$	1.45 @ 10	1.6	10	98.7	100	[7]
$Ni_{0.5}Co_{2.5}O_4$	1.53 @ 10	1.5	10	92.42	90.35	[8]
CuO-PdO	1.32 @ 10	1.35	10	96.2	93.7	[9]
$Ni(OH)_2$-NiOOH/NiFeP	1.35 @ 10	1.435	10	99	94	[10]
InOOH-O_v	1.34 @ 10	1.48	10	91.6	90.7	[11]
Ce–CoP	1.30 @ 10	1.44	10	98	96.4	[12]
S,N-MOFs@$Ni(OH)_2$-NSs/NF	1.32 @10	1.4	10	100	100	[13]
NiCu NTs	1.35@ 20	1.424	20	99	96.4	[14]
VN/NiF	1.36@ 10	1.38	10	96	84	[15]
WO_3/Ni	1.40@ 5	1.44	5	88.3	88	[16]
CoOOH	1.40@10	1.56	5	35.1	35.1	[17]
CoOOH	1.335@20	1.423	10	100	100	[18]

REFERENCES

[1] N. Zhang, Y. Zou, L. Tao, et al. Electrochemical Oxidation of 5-Hydroxymethylfurfural on Nickel Nitride/Carbon Nanosheets: Reaction Pathway Determined by In Situ Sum Frequency Generation Vibrational Spectroscopy. *Angew. Chem., Int. Ed.* 2019; 58: 15895-15903. https://doi.org/10.1002/anie.201908722

[2] Y. Lu, C.L. Dong, Y.C. Huang, et al. Identifying the Geometric Site Dependence of Spinel Oxides for the Electrooxidation of 5-Hydroxymethylfurfural. *Angew. Chem., Int. Ed.* 2020; 59: 19215-19221. https://doi.org/10.1002/anie.202007767

[3] Y. Lu, T. Liu, C.L. Dong, et al. Tuning the Selective Adsorption Site of Biomass on Co_3O_4 by Ir Single Atoms for Electrosynthesis. *Adv. Mater.* 2021; 33: e2007056. https://doi.org/10.1002/adma.202007056

[4] M. Zhang, Y.Q. Liu, B.Y. Liu, et al. Trimetallic NiCoFe-Layered Double Hydroxides Nanosheets Efficient for Oxygen Evolution and Highly Selective Oxidation of Biomass-Derived 5-Hydroxymethylfurfural. *ACS Catal.* 2020; 10: 5179-5189. https://doi.org/10.1021/acscatal.0c00007

[5] K. Gu, D. Wang, C. Xie, et al. Defect-Rich High-Entropy Oxide Nanosheets for Efficient 5-Hydroxymethylfurfural Electrooxidation. *Angew. Chem., Int. Ed.* 2021; 60: 20253-20258. https://doi.org/10.1002/anie.202107390

[6] Y. Lu, T. Liu, C.L. Dong, et al. Tailoring Competitive Adsorption Sites by Oxygen-Vacancy on Cobalt Oxides to Enhance the Electrooxidation of Biomass. *Adv. Mater.* 2022; 34: e2107185. https://doi.org/10.1002/adma.202107185

[7] X. Pang, H. Bai, H. Zhao, W. Fan, W. Shi. Efficient Electrocatalytic Oxidation of 5-Hydroxymethylfurfural Coupled with 4-Nitrophenol Hydrogenation in a Water System. *ACS Catal.* 2022; 12: 1545-1557. https://doi.org/10.1021/acscatal.1c04880

[8] Y. Lu, T. Liu, Y.-C. Huang, et al. Integrated Catalytic Sites for Highly Efficient Electrochemical Oxidation of the Aldehyde and Hydroxyl Groups in 5-Hydroxymethylfurfural. *ACS Catal.* 2022; 12: 4242-4251. https://doi.org/10.1021/acscatal.2c00174

[9] P. Zhou, X.S. Lv, S.S. Tao, et al. Heterogeneous-Interface-Enhanced Adsorption of Organic and Hydroxyl for Biomass Electrooxidation. *Adv. Mater.* 2022; 34: 9. https://doi.org/10.1002/adma.202204089

[10] R.P. Luo, Y.Y. Li, L.X. Xing, et al. A dynamic Ni(OH)-NiOOH/NiFeP heterojunction enabling high-performance E-upgrading of hydroxymethylfurfural. *Appl. Catal. B-Environ.* 2022; 311: 121357. https://doi.org/10.1016/j.apcatb.2022.121357

[11] F. Ye, S. Zhang, Q. Cheng, et al. The role of oxygen-vacancy in bifunctional indium oxyhydroxide catalysts for electrochemical coupling of biomass valorization with CO_2 conversion. *Nat. Commun.* 2023; 14: 2040. https://doi.org/10.1038/s41467-023-37679-3

[12] J.H. Bi, H. Ying, H. Xu, et al. Phosphorus vacancy-engineered Ce-doped CoP nanosheets for the electrocatalytic oxidation of 5-hydroxymethylfurfural. *Chem. Commun.* 2022; 58: 7817-7820. https://doi.org/10.1039/d2cc02451a

[13] D.D. Wang, W.B. Gong, J.F. Zhang, et al. In situ growth of MOFs on $Ni(OH)_2$ for efficient electrocatalytic oxidation of 5-hydroxymethylfurfural. *Chem. Commun.* 2021; 57: 11358-11361. https://doi.org/10.1039/d1cc04680b

[14] L.X. Zheng, Y.J. Zhao, P.H. Xu, et al. Biomass upgrading coupled with H_2 production via a nonprecious and versatile Cu-doped nickel nanotube electrocatalyst. *J. Mater. Chem. A* 2022; 10: 10181-10191. https://doi.org/10.1039/d2ta00579d

[15] S. Li, X. Sun, Z. Yao, et al. Biomass Valorization via Paired Electrosynthesis Over Vanadium Nitride-Based Electrocatalysts. *Adv. Funct. Mater.* 2019; 29: 1904780. https://doi.org/10.1002/adfm.201904780

[16] K. Hu, M. Zhang, B.Y. Liu, et al. Efficient electrochemical oxidation of 5-hydroxymethylfurfural to 2,5-furandicarboxylic acid using the facilely synthesized 3D porous WO_3/Ni electrode. *Mol. Catal.* 2021; 504: 8. https://doi.org/10.1016/j.mcat.2021.111459

[17] B.J. Taitt, D.H. Nam, K.S. Choi. A Comparative Study of Nickel, Cobalt, and Iron Oxyhydroxide Anodes for the Electrochemical Oxidation of 5-Hydroxymethylfurfural to 2,5-Furandicarboxylic Acid. *ACS Catal.* 2019; 9: 660-670. https://doi.org/10.1021/acscatal.8b04003

[18] R.Y. Zhang, S.H. Jiang, Y. Rao, et al. Electrochemical biomass upgrading on CoOOH nanosheets in a hybrid water electrolyzer. *Green Chem.* 2021; 23: 2525-2530. https://doi.org/10.1039/d0gc04157b